Palaeontology
The Palaeontological Association
Registered Charity No. 11683330

Oldest fossil ciliates from the Cryogenian glacial interlude reinterpreted as possible red algal spores

Journal:	*Palaeontology*
Manuscript ID	PALA-12-19-4665-OA.R2
Manuscript Type:	Original Article
Date Submitted by the Author:	16-Apr-2020
Complete List of Authors:	Cohen, Phoebe; Williams College, Geosciences; Williams College Vizcaino, Maoli; Williams College, Geosciences Anderson, Ross; University of Oxford, All Souls College; University of Oxford, Earth Sciences
Key words:	Mongolia, Neoproterozoic, Proterozoic, Taishir Formation, Cryogenian, microfossil

Oldest fossil ciliates from the Cryogenian glacial interlude reinterpreted as possible red algal spores

PHOEBE A. COHEN[1*], MAOLI VIZCAÍNO[1], *and* ROSS P. ANDERSON[2]

[1]Department of Geosciences, Williams College, Williamstown, MA USA; emails: pac3@williams.edu, maolivizcaino9@gmail.com

[2]All Souls College, University of Oxford, Oxford, OX1 4AL, UK; email: ross.anderson@all-souls.ox.ac.uk

[*] Corresponding author

Abstract: The Cryogenian Period experienced two long lived global glaciations known as Snowball Earths. While these events were dramatic, eukaryotic life persisted through them, and fossil evidence shows that eukaryotes thrived during the ca. 30-million-year interlude between the glaciations. Carbonate successions have become an important taphonomic window for this interval. One of the most notable examples is the ca. 662–635 Ma Taishir Formation (Tsagaan Olom Group, Zavkhan Terrane, Mongolia) which has yielded a number of eukaryotic fossil taxa. Here, we examine more closely the morphology and taxonomic affinity of some of these Taishir fossils previously interpreted as remains of ciliate tintinnid loricae (purportedly the oldest fossil ciliates). New morphological and ultrastructural analyses indicate that these fossils are not ciliate tintinnids. Instead, we propose a new interpretation: that they are algal reproductive structures related to coeval macroscopic organic warty sheets described as putative red algae. We report the first occurrence of these fossils in the earliest Ediacaran Ol Formation, indicating that this taxon persisted through the Marinoan Snowball Earth. A new interpretation of these fossils as putative

red algal spores has broad implications for our understanding of biodiversity in the Neoproterozoic Era, specifically during the Cryogenian Period, and for the antiquity of ciliates.

Keywords: Neoproterozoic, microfossil, Mongolia, Taishir Formation

STRATA from the Cryogenian non-glacial interlude (660 Ma – 640 Ma; Rooney et al., 2015) contain a small but important cohort of eukaryotic fossils (Bosak *et al.* 2011*a*, *b*; Dalton *et al.* 2013; Riedman 2014; Cohen *et al.* 2015; Ye *et al.* 2015; Moore *et al.* 2017). These fossils have greatly increased our understanding of life between the Sturtian (717–660 Ma) and Marinoan (~640–635 Ma) Snowball Earth glaciations. However, many of these fossils are difficult to interpret due to limited morphological features, lack of similarity to modern groups, and diagenetic issues that mask original features (e.g. Anderson *et al.* 2013).

Fossils from limestones of the Taishir Formation (Tsagaan Olom Group, Zavkhan Terrane, Mongolia) were originally interpreted by Bosak *et al.* (2011*c*) as codonellid tintinnid ciliates—the oldest example of this major eukaryotic group known—based on their external morphology; we refer to these fossils here as organic spore-like microfossils (OSM). However, a closer examination of tintinnid morphology shows that OSM share fewer characteristics with the ciliate clade, casting doubt on this interpretation. For example, extant tintinnids do not have central invaginations as many OSM do, rather, their loricae open in wide collars (Agatha and Simon 2012; Lipps *et al.* 2013). In addition, OSM have other shape variations that are inconsistent with extant tintinnids; thus, some doubt exists as to their taxonomic affinity. Various authors have argued that there is no concrete body fossil evidence of ciliates until at least the Ordovician Period if not later, suggesting alternative interpretations for OSM found in the Tsagaan Olom Group as well as for other putative tintinnid fossils found in Doushantuo

phosphates of South China (Li *et al.* 2007; Dunthorn *et al.* 2010; 2015). A better understanding of these enigmatic fossils is vital to dating the antiquity of eukaryotic clades, calibrating molecular clocks, and reconstructing ecosystems during the Cryogenian Period—a time with the most extreme climates in Earth history that forms the backdrop to the origination of metazoans (Erwin *et al.* 2011; Betts *et al.* 2018).

In addition to OSM, Cohen *et al.* (2015) described macroscopic organic warty sheets (MOWS) from Taishir limestones (Fig. 1A,B). Cohen *et al.* interpreted MOWS as putative marine red algae based on ultrastructural and morphology similarities. MOWS are sheet-like with raised, warty structures on one surface, similar to many crustose and blade-forming modern red algae within the Florideophyceae. When cut in half and viewed in cross section, the wart-like structures on MOWS are filled with organic material and cellular structures, which Cohen *et al.,* (2015) interpreted as reproductive structures similar to cystocarps seen in extant red algal groups (Fig. 2 A,B, E). Based on new morphological and ultrastructural data presented here, we reinterpret OSM as having the same origin as those structures preserved inside the warts of MOWS, thus indicating that they are not tinitinnid loricae but instead are a part of the MOWS organism and thus may be red algal spores.

GEOLOGICAL SETTING

The Cryogenian Period is represented in southwestern Mongolia by the Maikhan Ul, Taishir, and Khongor Formations of the Tsagaan Olom Group on the Zavkhan Terrane (Fig. 3) (Bold et al., 2016). The Maikhan Ul Formation is correlated to the Sturtian Snowball Earth, while the Khongor Formation is correlated to the Marinoan Snowball (Macdonald *et al.* 2009; Macdonald 2011; Rooney *et al.* 2015; Bold *et al.* 2016). The intervening Taishir Formation is split into 4 members over its 300–600 m thickness (Bold *et al.* 2016). Onset of Taishir deposition

is constrained by a Re-Os date of 659 ± 3.9/4.5 Ma (Rooney et al., 2015), and its lowest member T1 comprises a post-Sturtian cap carbonate containing nodular cherts (Bold *et al.* 2016; Lau *et al.* 2017). T2 begins as limestone calcisiltite, before pure carbonate layers that contain large <1cm ooids. T3 begins with limestone interbedded by debris flows and chert nodules, before massive black carbonate mudstones. T4 overlays T3 with limestone micrite and black shale. Bold *et al.* (2016) suggest that the Taishir Formation was deposited on an isolated platform, and that carbonate ramp morphology was promoted by the drowning of the lower T1 and T2 members. Then during the deposition of T3, ramp morphology began to shape into an outer rim.

Following the Marinoan-equivalent glacial Khongor Formation, the Ol Formation signifies the beginning of the Ediacaran Period (Fig. 3). At its base is a cap dolostone that ranges from 10–35m and shares sedimentological and geochemical characteristics with Marinoan cap carbonates globally (Bold et al., 2016; Macdonald, 2011; Macdonald et al., 2009). The Ol Formation varies from carbonate- to siliciclastic-dominated; Bold *et al.* (2016) suggest a mid-inner-ramp depositional environment.

MATERIALS AND METHODS

Carbonate rock samples were collected in 2013 and 2014 from the Taishir and Ol formations at Khongor (96º18 E, 46º40'N) and Taishir (96º36'E, 46º40'N), and studied in combination with Taishir Formation fossils previously described by Bosak *et al.* (2011c). New rock samples were washed and crushed into pea-sized pieces, and dissolved in 20% acetic acid. Acid-insoluble residues were rinsed with deionized water through a 25 μm sieve, and this fraction was dried on glass slides for examination via light microscopy. Microfossils were hand-picked from slides, transferred to scanning electron microscope (SEM) stubs, and coated with Pt/Pd, before being

imaged with a FEI Quanta 400 SEM. Morphological measurements were made using ImageJ software. Some OSM and MOWS were also embedded in epoxy, sectioned with a microtome, and imaged on glass slides with transmitted light in order to observe fossil cross sections; some cross-section measurements were focus stacked using Helicon Focus software. All statistical analyses were performed using R. All new rock samples are deposited in the Yale Peabody Museum under numbers YPM IP 547715.X- YPM IP 547720.X.

RESULTS

Fossil distributions

Of the ~200 stratigraphic horizons within the Taishir and Ol formation from which samples derive, 30 yielded OSM and 18 yielded MOWS (Fig. 3; *Cohen et al. 2020*). OSM and MOWS both appear in all three members sampled of the Cryogenian Taishir Formation. OSM also appear in the Ediacaran Ol Formation, but MOWS do not. OSM only occur in one sample of T1, but this sample was pooled from multiple taken over ~15 meters of stratigraphy, so it is difficult to ascertain how many horizons within that interval contained OSM (Bosak *et al.* 2011c). Interestingly, only one hand sample, from T2, contains both OSM and MOWS (Bosak *et al.* 2011c).

Fossil morphology

OSM can be flask-shaped, rectangular, or tapered yet all share similar size distributions, a width to length ratio less than 1, leathery bulbous surface textures, and are composed of organic carbon (Fig. 4, Fig 5A, Fig 6). Many OSM exhibit spherical structures on their surfaces interpreted by Bosak *et al.* (2011) as alveoli similar to those found on the tests of some modern

tintinnids (Fig. 4E). The mean end diameter of OSM is 41.7 μm (sd 15.7 μm, N=67) and the mean length is 76 μm (sd 21 μm, N=67). Despite their varied morphologies, histograms of length and diameter show continuous distributions, indicating that OSM are a single population (Fig 6). We did observe some differences in diameter and length of OSM between fossiliferous sections (Table 2, Figure 7; T1 excluded due to the fact that only one grouped sample contains OSM) but as two of our sections have limited numbers of measured samples we hesitate to draw conclusions from these differences

Qualitatively, the ends of OSM are very similar to the tops of wart-like structures on MOWS (Fig. 1B,C, Fig. 5A,B). The tops of warts of MOWS are circular, slightly depressed relative to the rest of the wart structure, and have a leathery texture, much like the ends of OSM. Quantitatively, a Welch two sample t-test on the end diameters of OSM (N=67) and the tops of MOWS warts (N=41) produced a p value of 0.87 with a 95% confidence interval range of -4.42–3.76indicating that the mean diameters are not significantly different (Table 1).

Fossil microstructure

Similarities between OSM and MOWS extend to their internal morphology. Micrographs of cross-sectioned OSM reveal that the spherical structures seen in many SEM images are not solely external forms, but are present internally as well, filling the entire OSM structure and resembling cellular material (Fig. 2C,D). Cross sections of the warts of MOWS have similar spherical structures (Fig. 2A,B). A Welch two sample t-test on the diameters of these spherical cell-like structures in OSM (N=85) and warts of MOWS (N=25) produced a p-value of 0.19 with a 95% confidence interval range of -0.14–0.68 indicating that the mean diameters are not significantly different (Table 1).

DISCUSSION

OSM are not ciliates

Our microstructural analysis of OSM is inconsistent with a purported affinity to ciliate tintinnid loricae. While the walls of tintinnid loricae can consist of repeating circular shapes, these shapes are on the sub-micron scale, and thus much smaller than the cellular structures seen in sections of OSM (Agatha *et al.* 2012). Moreover, the internal portion of the loricae are hollow save the single-celled organism itself (Fig. 2F, Fig 5D, Agatha *et al.* 2013). During reproduction, tintinnid loricae can fill with smaller cells, but this is a short-lived stage and cells are not reinforced by any substantial connective biopolymer, thus it is highly unlikely that this stage would be repeatedly preserved. In addition, the cells in this stage are still distinct from the lorica itself and don't interact with the outer wall as seen in OSM (Agatha *et al.* 2012). Thus, if these stages were preserved, we would expect to see a distinct lorica wall surrounding less robust cellular material. In summary, the microstructure of tintinnid loricae do not show a consistent pattern of homogeneous repeating cellular material throughout the entirety of the structure like the OSM studied here (Agatha and Simon, 2012; Agatha *et al.* 2012). In contrast, OSM and the internal wart material of MOWS share both external and internal morphology including overall size, shape, and the nature of their internal cellular material. Thus, we instead argue that OSM and the warts of MOWS share an origin (Fig. 5).

Our removal of OSM from the ciliate fossil record is consistent with the nature of their remaining fossil record, which is generally poor (Lipps et al 2013). Fossils of tintinnids are the best group to use for tracing the evolution of ciliates over time because their loricae provide higher preservation potential compared to other members of the ciliate group (Lipps *et al* 2013,

Dolan 2012). While tintinnid affinities have been claimed for rare fossils in Ordovician and Ediacaran strata (Li *et al.* 2007), conclusive well-accepted tintinnid fossils are not found before the Mesozoic Era (Lipps *et al.* 2013; Dunthorn *et al.* 2015). Our interpretation is also consistent with recent molecular clock analyses, which show that while ciliates likely diverged between 1,000 and 500 Ma, (Betts *et al.* 2018) tintinnids did not originate until between 351-191 Ma, well after the Cryogenian Period (Fernandes and Schrago 2019).

Are OSM Red Algal Spores?

If OSM are not tintinnids, then what other possible affinities exist for this group? Cohen *et al.* argued that MOWS are the remains of an unknown red algal fossil taxon. If this interpretation is correct, then OSM could be the remains of red algal spores or other reproductive structures, as Cohen *et al.* interpreted the warts as red algal reproductive cystocarps. While red algal reproduction is varied, the general sequence of events within the Florideophycea is that a female red algal gametophyte is fertilized by spermatozoa released by a male gametophyte, forming carposporophytes on the female gametophyte (Cole and Sheath, 1990; Fig 2E). The carposporophyte, which contains many fertilized carpospores, is contained in a structure called a pericarp; this entire structure is called a cystocarp (Fig. 5C), which Cohen *et al.* (2015) compared to the warts of MOWS. The carposporophyte releases carpospores which then eventually go on to produce new male and female gametophytes (Cole and Sheath 1990).

We suggest that MOWS represent the gametophye of a red alga, MOWS warts are cystocarps, and OSM are carposporophytes (Fig 5A, B, C). These assignments would indicate a bi-phasic life cycle for Cryogenian red algae. Red algae have the longest fossil record of any eukaryotic crown group, with convincing examples reaching back ca. 1.0 Ga (Butterfield 2000;

Gibson *et al.* 2017) and molecular clock divergence estimates between 1,200 and 800 Ma (Betts *et al.* 2018). Thus, both the fossil and molecular records indicate that red algae have been in existence at a minimum of ~300 million years before the appearance of OSM/MOWS, lending support to the taxonomic assignment.

We argue that a red algal affinity is also most parsimonious when considering other options (Table 3). We compared OSM/MOWS morphologies to those of all other comparable clades that either have a Neoproterozoic fossil record, or are inferred to have existed during Cryogenian time based on phylogenetic and molecular data (Parfrey *et al.* 2011; Cohen and Macdonald 2015). These include red algae, green algae, amoebozoa, rhizaria, fungi, and sponges. The attributes we considered were: crustose form, multicellularity, a bi-phasic life cycle, marine, warty protuberances on a single surface, and cellular material contained within warty protuberances. The green algae do not contain crustose forms, and no forms that we surveyed had warts (Graham and Wilcox 2000). Rhizaria and Amoebazoa do not form multicellular recalcitrant structures in their marine habitats (Lindley *et al.* 2007; Brown *et al.* 2012). Sponges can be crustose, and crustose forms have wart-like ostioles, but these are not filled with cellular material since they are used for water transport and filtration. Ascomycete fungi can have crustose forms with wart-like reproductive structures, but none are known from marine settings (Shearer *et al.* 2006). Transport, while possible, is unlikely given the wide variety of inferred water depth of the fossiliferous parts of the Taishir Formation and the lack of relationship between the basin's sequence stratigraphic architecture and the presence or absence of either type of fossil (Bold et al. 2016). Only the red algae contain all of the features found in the organism represented by OSM/MOWS. Despite these comparisons, we acknowledge that the assignment of MOWS to crown group red algae cannot be entirely conclusive due to a lack of

taxonomically diagnostic features such as pit connections (Cole and Sheath 1990), and that it is also possible that OSM/MOWS represent an extinct stem group with no modern descendants, making definitive comparisons impossible.

Explaining Stratigraphic Occurrence via Taphonomy

Puzzlingly if OSM and MOWS do represent parts of the same organism, they are only rarely reported from the same hand sample (Fig. 3). Taphonomic processes may explain the non-overlapping stratigraphic distribution; this explanation is valid for both a red algal interpretation as well as other taxonomic interpretations. When processing Taishir rocks to extract fossils, we noted that MOWS are generally more fragile and easily damaged during sample processing than OSM and that, when sectioned, the internal wart structures of MOWS appear to have much thicker and more robust organic walls than the external material of MOWS (Fig. 2A,B). This may be indicative of the relative resistance to decay of the different parts of the organism represented by OSM/MOWS. OSM may be more resistant to decay than MOWS given there thicker and more robust structure, Thus, during diagenesis, the external structure of MOWS could be degraded preferentially, leaving behind only OSM (Fig. 8). In areas of better preservation, MOWS with OSM still intact as warts are preserved, whereas in areas with poorer preservation, only OSM remain. This argument further discounts transport from a terrestrial setting as a source of the fossil material, because we would expect to find better preservation (i.e., MOWS) in shallower water settings, and poorer preservation (i.e., OSM) in deeper water settings, and this pattern is not observed in our data.

Implications for eukaryotic diversity and ecosystems

The discovery that OSM, originally interpreted as ciliates from the Cryogenian glacial interlude, are not ciliates and may in fact be red algal carposporophytes, renders the fossil record of ciliates equivocal until at least the Paleozoic Era (Streng *et al.* 2005). Our findings remove ciliates from the Cryogenian fossil record, and thus lower the known diversity of actual and inferred (range-through) Cryogenian crown group eukaryotes from 8 to 7 (Cohen and Macdonald 2015). Additionally, a ciliate affinity for OSM would have implied that these organisms were predatory (as all tintinnids are predatory grazers, and modern tintinnids feed on eukaryotic prey (Montagnes 2012)). They would represent a rare example of Cryogenian ecosystem complexity (Bosak *et al.* 2011c). While other evidence indicates that predation and eukaryvory were already common in the older Tonian Period (Cohen and Riedman 2018), our reinterpretation indicates that there is no *direct* fossil evidence for predation in Cryogenian ecosystems.

In addition, new Ediacaran OSM occurrences show that they persisted through the Marinoan Snowball Earth—the first well-defined fossil group to have a continuous fossil record across this tumultuous interval. While various acritarchs have fossil records in Tonian, Cryogenian, and Ediacaran strata e.g., *Leiospheridia* spp. (thus spanning both Cryogenian Snowball Earths; (Riedman and Sadler 2017)), their simple morphology renders them taxonomically ambiguous (e.g. Butterfield 2004) and thus we cannot be certain that these fossil records represent the survival and persistence of distinct biological entities. However, our findings demonstrate for the first time a single fossil group, possibly defined at the level of a genus, with a record directly bracketing the Marinoan glaciation - from both non-glacial interlude Cryogenian and earliest Ediacaran strata.

If the red algal interpretation for MOWS is correct then our discovery suggests the presence of at least a bi-phasic life cycle for Cryogenian red algae, which is consistent with the

multiple life stages identified in the ca. 1000 Ma crown group red algae *Bangiomorpha* (Butterfield 2000). This interpretation also has implications for the types of biological refugia necessary during Snowball Earths – the OSM/MOWS organism would have required sustained aquatic habitats where photosynthesis and spore transport were possible, which supports the idea that there were at least limited open-water ecosystems with access to sunlight (Ye *et al.* 2015).

CONCLUSIONS

Our work shows that OSM are not the oldest remains of tintinnid ciliates. Instead, we propose that they represent part of MOWS, and further propose that OSM and MOWS may represent components of a bi-phasic life cycle of an early red alga. This study emphasizes the importance of taking into consideration life cycles when interpreting Proterozoic fossils. Accurately interpreting enigmatic Proterozoic fossils is critical for reconstructing early eukaryotic ecosystems, calibrating molecular clocks used to determine clade antiquity, and determining how and where life persisted during Snowball Earth events.

Acknowledgements. PAC acknowledges support from the NASA Astrobiology Institute (NNA13AA90A) and Williams College and thanks N. Piatczyc for microscopy assistance and support. G. Markel for lab assistance, and R. Kodner and Z. Bernstein for manuscript feedback. MV acknowledges support from the Allison Davis Fellowship. RPA acknowledges support from the American Philosophical Society/NASA Lewis and Clark Fund in Astrobiology, a Geological Society of America ExxonMobil Student Geoscience Grant, NASA (NNA13AA90A and NNX14AP10H), and the Yale Institute for Biospheric Studies and Peabody Museum of Natural History. RPA thanks D. Briggs for support during this project. Fieldwork was facilitated by U.

Bold, F. Macdonald, and E. F. Smith, and supported by C. Dwyer, T. Killian, E. Smith, and students and staff of the Mongolian University of Science and Technology. S. Butts and J. Utrup managed collections. We thank P. Strother and two anonymous reviewers for their constructive comments.

DATA ARCHIVING STATEMENT

Data for this study are available in the Dryad Digital Repository: https://datadryad.org/stash/dataset/doi:10.5061/dryad.fn2z34tqx

REFERENCES CITED

AGATHA, S. and SIMON, P. 2012. On the Nature of Tintinnid Loricae (Ciliophora: Spirotricha: Tintinnina): a Histochemical, Enzymatic, EDX, and High-resolution TEM Study. *Acta Protozoologica*, **2012**, 1–19.

AGATHA, S., LAVAL PEUTO, M. and SIMON, P. 2012. The tintinnid lorica. *The biology and ecology of tintinnid ciliates: Models for marine plankton*, 17–41.

ANDERSON, R. P., FAIRCHILD, I. J., TOSCA, N. J. and KNOLL, A. H. 2013. Microstructures in metasedimentary rocks from the Neoproterozoic Bonahaven Formation, Scotland: Microconcretions, impact spherules, or microfossils? *Precambrian Research*, **233**, 59-72.

BETTS, H. C., PUTTICK, M. N., CLARK, J. W., WILLIAMS, T. A., DONOGHUE, P. C. J. and PISANI, D. 2018. Integrated genomic and fossil evidence illuminates life's early evolution and eukaryote origin. *Nature Ecology & Evolution*, **2**, 1556.

BOLD, U., SMITH, E. F., ROONEY, A. D., BOWRING, S. A., BUCHWALDT, R., DUDAS, F., RAMEZANI, J., CROWLEY, J. L., SCHRAG, D. P. and MACDONALD, F. A. 2016. Neoproterozoic stratigraphy of the Zavkhan terrane of Mongolia: The backbone for Cryogenian and early Ediacaran chemostratigraphic records. *American Journal of Science*, **316**, 1–63.

BOSAK, T., LAHR, D. J. G., PRUSS, S. B., MACDONALD, F. A., DALTON, L. and MATYS, E. 2011*a*. Agglutinated tests in post-Sturtian cap carbonates of Namibia and Mongolia. *Earth and Planetary Science Letters*, **308**, 29–40.

BOSAK, T., LAHR, D. J. G., PRUSS, S. B., MACDONALD, F. A., GOODAY, A. J., DALTON, L. and MATYS, E. D. 2011*b*. Possible early foraminiferans in post-Sturtian (716-635 Ma) cap carbonates. *Geology*, **40**, 67–70.

BOSAK, T., MACDONALD, F., LAHR, D. and MATYS, E. 2011*c*. Putative Cryogenian ciliates from Mongolia. *Geology*, **39**, 1123–1126.

BROWN, M. W., KOLISKO, M., SILBERMAN, J. D. and ROGER, A. J. 2012. Aggregative Multicellularity Evolved Independently in the Eukaryotic Supergroup Rhizaria. *Current Biology*, **22**, 1123–1127.

BUTTERFIELD, N. J. 2000. Bangiomorpha pubescens n. gen., n. sp.: implications for the evolution of sex, multicellularity, and the Mesoproterozoic/Neoproterozoic radiation of eukaryotes. *Paleobiology*, **26**, 386–404.

BUTTERFIELD, N. J. 2004. A vaucheriacean alga from the middle Neoproterozoic of Spitsbergen: implications for the evolution of Proterozoic eukaryotes and the Cambrian explosion. *Paleobiology*, **30**, 231–252.

COHEN, P.A., VIZCAINO, M., and ANDERSON, R. 2020. Oldest fossil ciliates from the Cryogenian glacial interlude reinterpreted as possible red algal spores. Dryad Digital Repository. https://doi.org/10.5061/dryad.fn2z34tqx

COHEN, P. A. and MACDONALD, F. A. 2015. The Proterozoic Record of Eukaryotes. *Paleobiology*, **41**, 610–632.

COHEN, P. A. and RIEDMAN, L. A. 2018. It's a protist-eat-protist world: recalcitrance, predation, and evolution in the Tonian–Cryogenian ocean. *Emerging Topics in Life Sciences*, **2**, 173–180.

COHEN, P. A., MACDONALD, F. A., PRUSS, S., MATYS, E. and BOSAK, T. 2015. Fossils of Putative Marine Algae from the Cryogenian Glacial Interlude of Mongolia. *PALAIOS*, **30**, 238–247.

COLE, K. M. and SHEATH, R. G. 1990. *Biology of the red algae*. Cambridge University Press.

DALTON, BOSAK, T., MACDONALD, F. A., LAHR, D. J. G. and PRUSS, S. B. 2013. Preservational and Morphological Variability of Assemblages of Agglutinated Eukaryotes in Cryogenian Cap Carbonates of Northern Namibia, *PALAIOS*, **28**, 67–79.

DUNTHORN, M., LIPPS, J. H. and STOECK, T. 2010. Reassessment of the Putative Ciliate Fossils Eotintinnopsis, Wujiangella, and Yonyangella from the Neoproterozoic Doushantuo Formation in China. *Acta Protozoologica*, **49**, 139–144.

DUNTHORN, M., LIPPS, J. H., DOLAN, J. R., SAAB, M. A.-A., AESCHT, E., BACHY, C., DE CAO, M. S. B., BERGER, H., BOURLAND, W. A., CHOI, J. K., CLAMP, J., DOHERTY, M., GAO, F., GENTEKAKI, E., GONG, J., HU, X., HUANG, J., KAMIYAMA, T., JOHNSON, M. D., KAMMERLANDER, B., KIM, S. Y., KIM, Y.-O., LA TERZA, A., LAVAL PEUTO, M., LIPSCOMB, D., LOBBAN, C. S., LONG, H., LUPORINI, P., LYNN, D. H., MACEK, M., MANSERGH, R. I., MARTÍN-CERECEDA, M., MCMANUS, G. G., MONTAGNES, D. J. S., ONG'ONDO, G. O., PATTERSON, D. J., PÉREZ-UZ, B., QUINTELA-ALONSO, P., SAFI, L. S. L., SANTOFERRARA, L. F., SONNTAG, B., SONG, W., STOECK, T., STOECKER, D. K., STRÜDER-KYPKE, M. C., TRAUTMANN, I., UTZ, L. R. P., VALLESI, A., VDACNY, P., WARREN, A., WEISSE, T., WICKHAM, S. A., YI, Z., ZHANG, W., ZHAN, Z., ZUFALL, R. and AGATHA, S. 2015. Ciliates — Protists with complex morphologies and ambiguous early fossil record. *Marine Micropaleontology*, **119**, 1–6.

ERWIN, D. H., LAFLAMME, M., TWEEDT, S. M., SPERLING, E. A., PISANI, D. and PETERSON, K. J. 2011. The Cambrian Conundrum: Early Divergence and Later Ecological Success in the Early History of Animals. *Science,* **334**, 1091–1097.

FERNANDES, N. M. and SCHRAGO, C. G. 2019. A multigene timescale and diversification dynamics of Ciliophora evolution. *Molecular Phylogenetics and Evolution*, **139**, 106521.

GIBSON, T. M., SHIH, P. M., CUMMING, V. M., FISCHER, W. W., CROCKFORD, P. W., HODGSKISS, M. S. W., WÖRNDLE, S., CREASER, R. A., RAINBIRD, R. H., SKULSKI,

T. M. and HALVERSON, G. P. 2017. Precise age of Bangiomorpha pubescens dates the origin of eukaryotic photosynthesis. *Geology*, **46**, 135–138.

GRAHAM, L. E. and WILCOX, L. W. 2000. Algae. *NJ Prentice Hall*, 640 pp.

LAU, K. V., MACDONALD, F. A., MAHER, K. and PAYNE, J. L. 2017. Uranium isotope evidence for temporary ocean oxygenation in the aftermath of the Sturtian Snowball Earth. *Earth and Planetary Science Letters*, **458**, 282–292.

LI, C. W., CHEN, J. Y., LIPPS, J. H., GAO, F., CHI, H. M. and WU, H. J. 2007. Ciliated protozoans from the Precambrian Doushantuo Formation, Wengan, South China. *Geological Society, London, Special Publications*, **286**, 151–156.

LINDLEY, L. A., STEPHENSON, S. L. and SPIEGEL, F. W. 2007. Protostelids and myxomycetes isolated from aquatic habitats. *Mycologia*, **99**, 504–509.

LIPSS, J. H., STOECK, T., & DUNTHORN, M., 2013, Fossil tintinnids. *in* Dolan, J.R.,. Montagnes, D.J.S., Agathat, S., Coates, D.W., and Stoecker, D.K. eds., The biology and ecology of tintinnid ciliates: models for marine plankton. Wiley-Blackwell, West Sussex, p. 186-197

MACDONALD, F. A. 2011. Chapter 29 The Tsagaan Oloom Formation, southwestern Mongolia. *Geological Society, London, Memoirs*, **36**, 331–337.

MACDONALD, F. A., JONES, D. S. and SCHRAG, D. P. 2009. Stratigraphic and tectonic implications of a newly discovered glacial diamictite-cap carbonate couplet in southwestern Mongolia. *Geology*, **37**, 123–126.

MONTAGNES, D. J. 2012. Ecophysiology and behavior of tintinnids. *in* Dolan, J.R.,. Montagnes, D.J.S., Agathat, S., Coates, D.W., and Stoecker, D.K. eds., The biology and ecology of tintinnid ciliates: models for marine plankton. Wiley-Blackwell, West Sussex, p., 85–121.

MOORE, K. R., BOSAK, T., MACDONALD, F. A., LAHR, D. J. G., NEWMAN, S., SETTENS, C. and PRUSS, S. B. 2017. Biologically agglutinated eukaryotic microfossil from Cryogenian cap carbonates. *Geobiology*, **15**, 499-515.

PARFREY, L. W., LAHR, D. J., KNOLL, A. H. and KATZ, L. A. 2011. Estimating the timing of early eukaryotic diversification with multigene molecular clocks. *Proceedings of the National academy of Sciences of the United States of America*, **108**, 13624–13629.

R CORE TEAM. 2017. R: A language and environment for statistical computing. R Foundation for Statistical Computing, Vienna, Austria. URL https://www.R-project.org/.

RIEDMAN, L. A. 2014. Organic-walled microfossil assemblages from glacial and interglacial Neoproterozoic units of Australia and Svalbard. *Geology*, **42**, 1011-1014.

RIEDMAN, L. A. and SADLER, P. M. 2017. Global species richness record and biostratigraphic potential of early to middle Neoproterozoic eukaryote fossils. *Precambrian Research*, **319**, 6-18.

ROONEY, A. D., STRAUSS, J. V., BRANDON, A. D. and MACDONALD, F. A. 2015. A Cryogenian chronology: Two long-lasting synchronous Neoproterozoic glaciations. *Geology*, **43**, 459-462.

SHEARER, C. A., DESCALS, E., KOHLMEYER, B., KOHLMEYER, J., MARVANOVÁ, L., PADGETT, D., PORTER, D., RAJA, H. A., SCHMIT, J. P., THORTON, H. A. and VOGLYMAYR, H. 2006. Fungal biodiversity in aquatic habitats. *Biodiversity and Conservation*, **16**, 49–67.

STRENG, M., BABCOCK, L. E. and HOLLINGSWORTH, J. S. 2005. AGGLUTINATED PROTISTS FROM THE LOWER CAMBRIAN OF NEVADA. *Journal of Paleontology*, **79**, 1214–1218.

URIÓSTEGUI, A. G., JIMÉNEZ, P. G., MARIÁN, F., ROBLEDO, D. and ROBAINA, R. 2002. Polyamines influencing maturation in reproductive structures of *Gracilaria Cornea* (Gracilariales, Rhodophyta) *Journal of Phycology*, **38**, 1169–1175.

YE, Q., TONG, J., XIAO, S., ZHU, S., AN, Z., TIAN, L. and HU, J. 2015. The survival of benthic macroscopic phototrophs on a Neoproterozoic snowball Earth. *Geology*, **43**, 507–510.

Figure Captions

FIG 1. Morphological and ultrastructural comparison of MOWS and OSM. A, MOWS individual from F864-20 (T2) with wart structures. B, Wart top of MOWS closeup from RPA 1301 (T2). C, OSM individual from YPM IP 547718.1 (Ol Fm) showing end of specimen. Scale bar in A is 125 μm, 12μm in B, 15μm in C.

FIG 2. A, B, Sectioned wart from MOWS from YPM IP 547715.1 (T2) Note pale colour of surrounding MOWS material. C, D, Sectioned OSM individual from YPM IP 547718.1 (Ol Fm). E, Modern red algal carposporangia (Urióstegui *et al.* 2002). F, Modern tintinnid *Favella ehrenbergii* (Agatha *et al.* 2012). Note that E and F are approximately an order of magnitude larger than A-D. Scale bar in A is 25μm in A and B, 30μm in C, 35μm in D, 200μm in E, and 100 μm in F.

FIG 3. Stratigraphy of the Khongor and Taishir localities showing distribution of fossils. Stratigraphy modified from Bold *et al.* 2016. MU= Maikhan-Uul Formation; K= Khongor Formation. See Cohen *et al.* 2020 for detailed sample and locality data and Bold *et al*. 2016 for geological maps.

FIG 4. Images of OSM. A, SEM image of YPM IP 547718.2A (Ol Fm). B, SEM image of OSM from YPM IP 547718.9A (Ol Fm). C, SEM image of OSM from YPM IP 547715.2A (T2). D, OSM from YPM IP 547718.2A (Ol Fm). E, SEM image of OSM from YPM IP 547718.9B (Ol Fm), arrow points to spherical surface structures on end of fossil. F, SEM image of end of an OSM YPM IP 547716.1A (T2), showing surface texture. G, OSM individual from YPM IP 547715.2 (T2), viewed in regular white transmitted light, showing dense organic material. Scale bar is 30µm in A, B, D, G; 35µm in C &E, and 80µm in F.

FIG 5. Diagram of structures described in the text. A, OSM showing spherical structures, and dimensions measured. B, MOWS showing wart, internal spherical structures, and wart top diameter measured in comparison to OSM diameter. C, Red algal cystocarp showing carpospores clustered together in a carposporophyte, surrounded by pericarp and sitting on top of / adjacent to gametophyte tissue. D, Tintinnid showing lorica, lorica wall, and single-celled organism inside lorica.

FIG 6. Histograms of OSM lengths and diameters showing continuous distributions.

FIG. 7. Boxplot showing comparison of lengths and widths of OSM from each member examined in this study.

FIG 8. Diagram of potential mechanisms of OSM/MOWS formation and dispersal. 1, External tissues are degraded, leaving behind 2, the internal cellular material as an OSM individual. 3, Carpospores are released, but do not preserve or are lost in sample processing in 4.

TABLE 1. Measurements of fossil material

TABLE 2. Comparison of fossil measurements in stratigraphic sections

TABLE 3. Comparison of possible affinities for OSM/MOWS

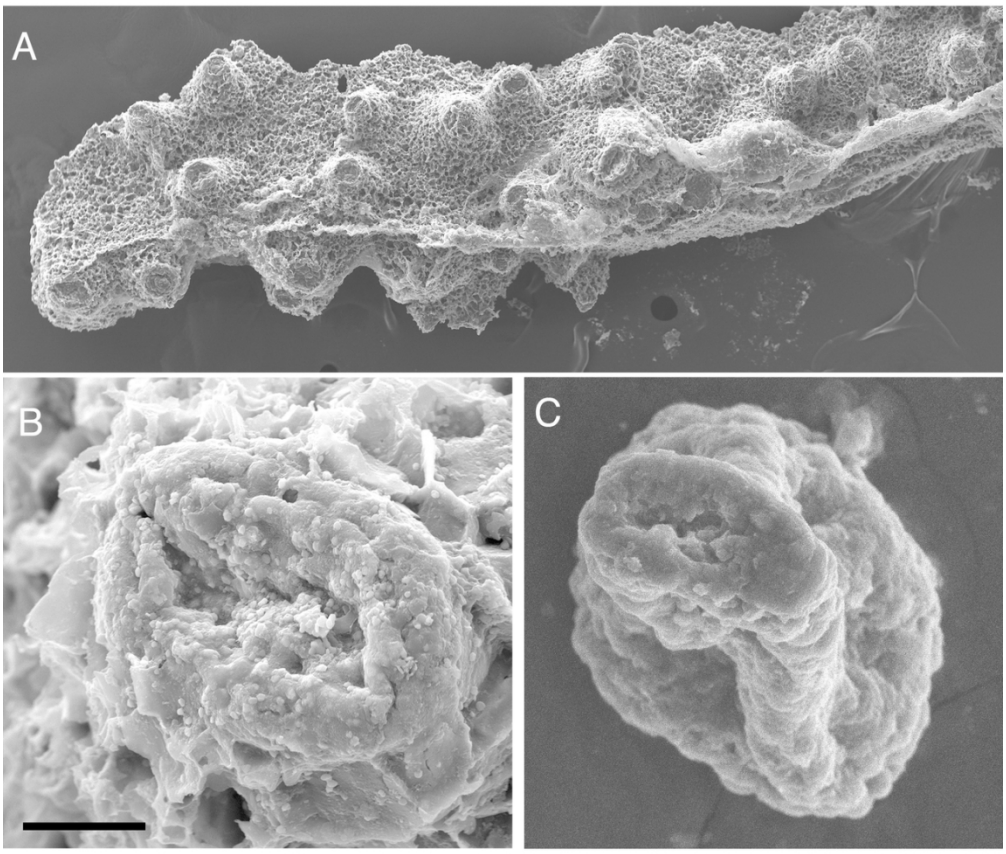

FIG 1. Morphological and ultrastructural comparison of MOWS and OSM. A, MOWS individual from F864-20 (T2) with wart structures. B, Wart top of MOWS closeup from RPA 1301 (T2). C, OSM individual from YPM IP 547718.1 (Ol Fm) showing end of specimen. Scale bar in A is 125 μm, 12μm in B, 15μm in C.

109x94mm (300 x 300 DPI)

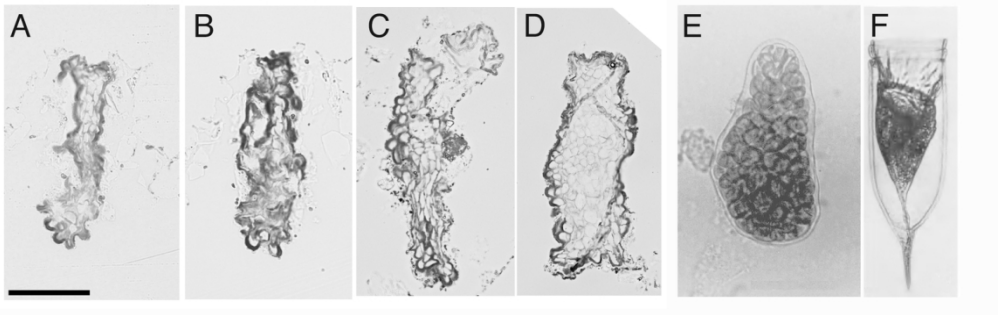

FIG 2. A, B, Sectioned wart from MOWS from YPM IP 547715.1 (T2) Note pale colour of surrounding MOWS material. C, D, Sectioned OSM individual from YPM IP 547718.1 (Ol Fm). E, Modern red algal carposporangia (Urióstegui et al. 2002). F, Modern tintinnid Favella ehrenbergii (Agatha et al. 2012). Note that E and F are approximately an order of magnitude larger than A-D. Scale bar in A is 25μm in A and B, 30μm in C, 35μm in D, 200μm in E, and 100 μm in F.

132x42mm (300 x 300 DPI)

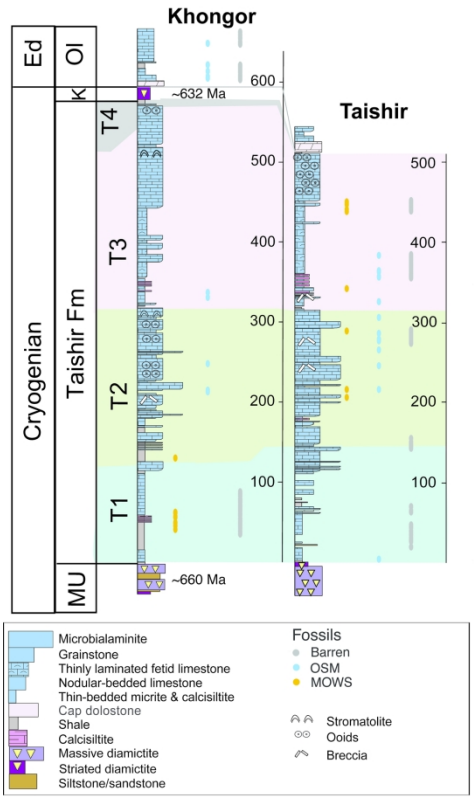

FIG 3. Stratigraphy of the Khongor and Taishir localities showing distribution of fossils. Stratigraphy modified from Bold et al. 2016. MU= Maikhan-Uul Formation; K= Khongor Formation. See Cohen et al. 2020 for detailed sample and locality data and Bold et al. 2016 for geological maps.

108x275mm (300 x 300 DPI)

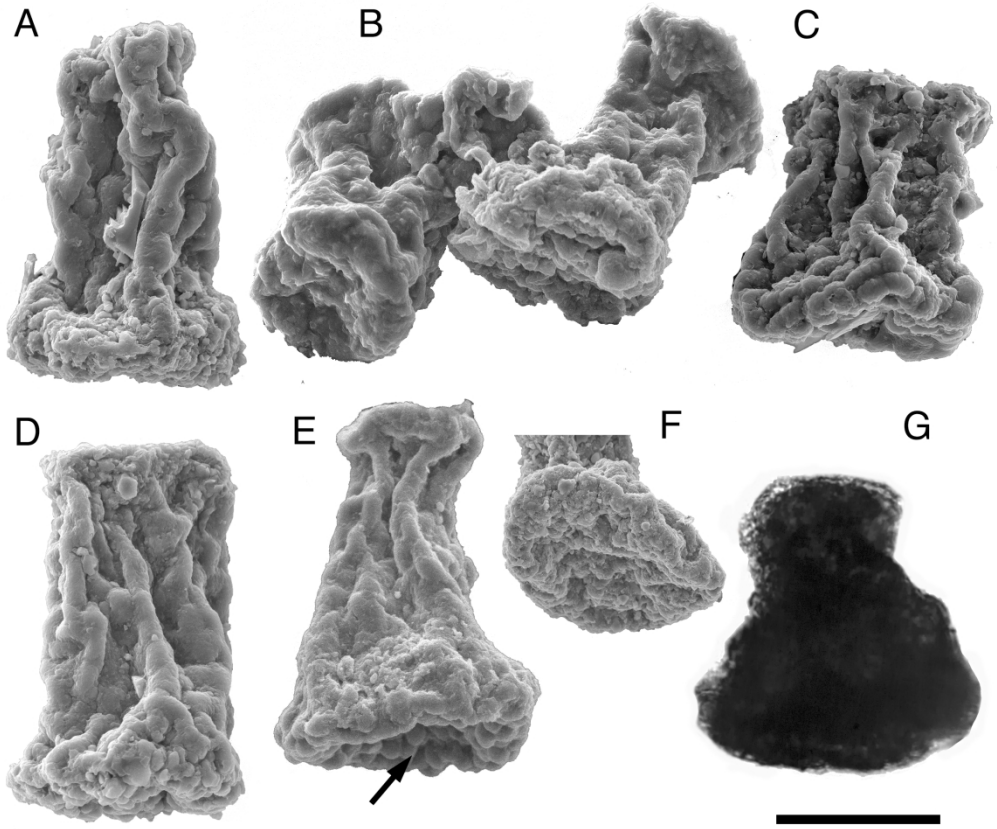

FIG 4. Images of OSM. A, SEM image of OSM from RPA1402_1.95 (Ol Fm). B, , SEM image of OSM from RPA1402_43.85 (Ol Fm). C, , SEM image of OSM from RPA1301_24 (T2). D, OSM from RPA1402_1.95 (Ol Fm). E, , SEM image of OSM from RPA1402_43.85 (Ol Fm), arrow points to spherical surface structures on end of fossil. F, , SEM image of end of an OSM individual, RPA1302_5 (T2), showing surface texture. G. OSM individual from RPA1301_24 (T2), viewed in regular white transmitted light, showing dense organic material. Scale bar is 30μm in A, B, D, G; 35μm in C &E, and 80μm in F.

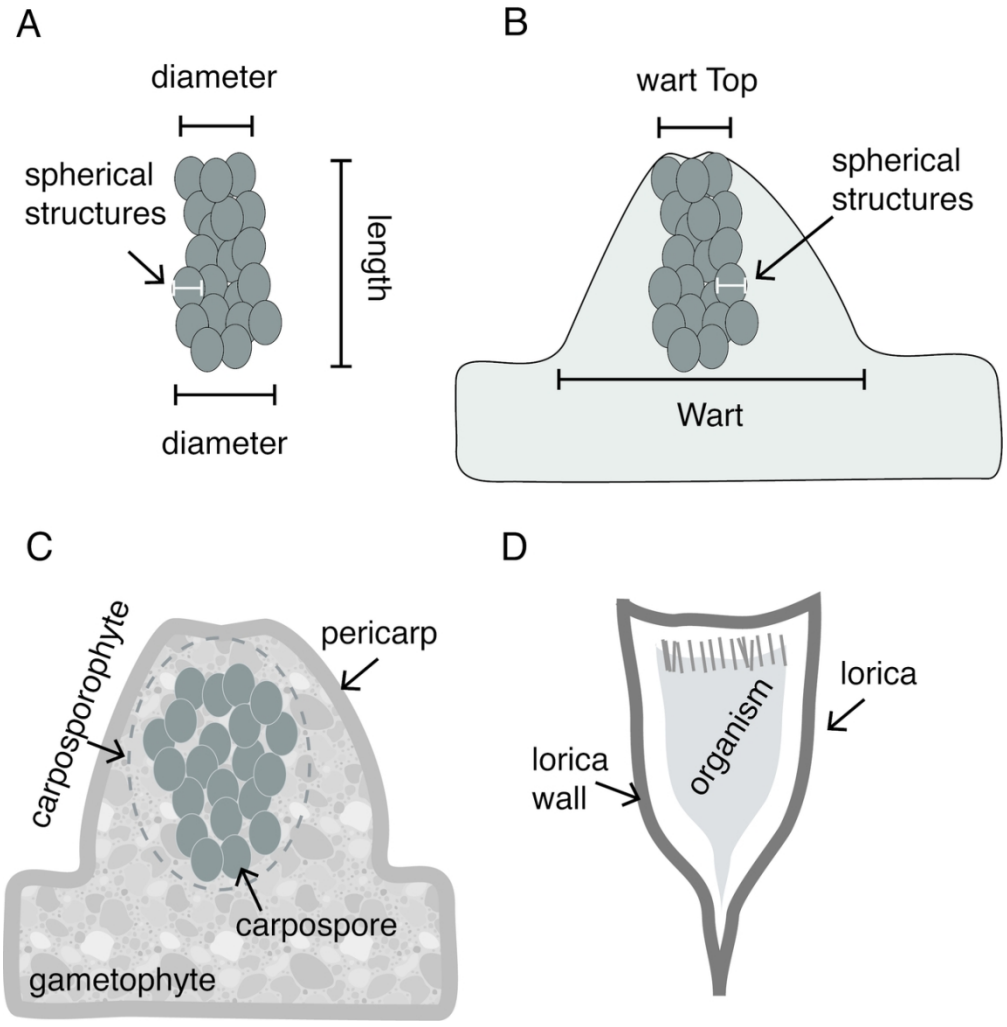

FIG 5. Diagram of structures described in the text. A, OSM showing spherical structures, and dimensions measured. B, MOWS showing wart, internal spherical structures, and wart top diameter measured in comparison to OSM diameter. C, Red algal cystocarp showing carpospores clustered together in a carposporophyte, surrounded by pericarp and sitting on top of / adjacent to gametophyte tissue. D, Tintinnid showing lorica, lorica wall, and single-celled organism inside lorica.

108x110mm (300 x 300 DPI)

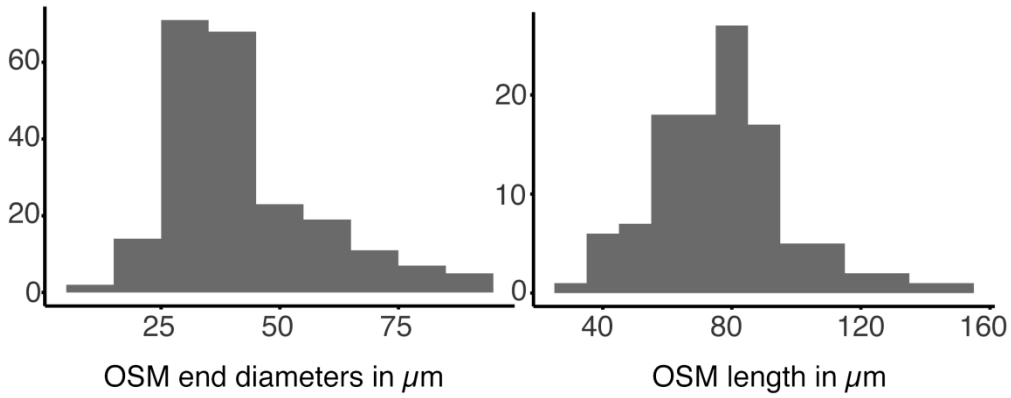

Histograms of OSM lengths and diameters showing continuous distributions.

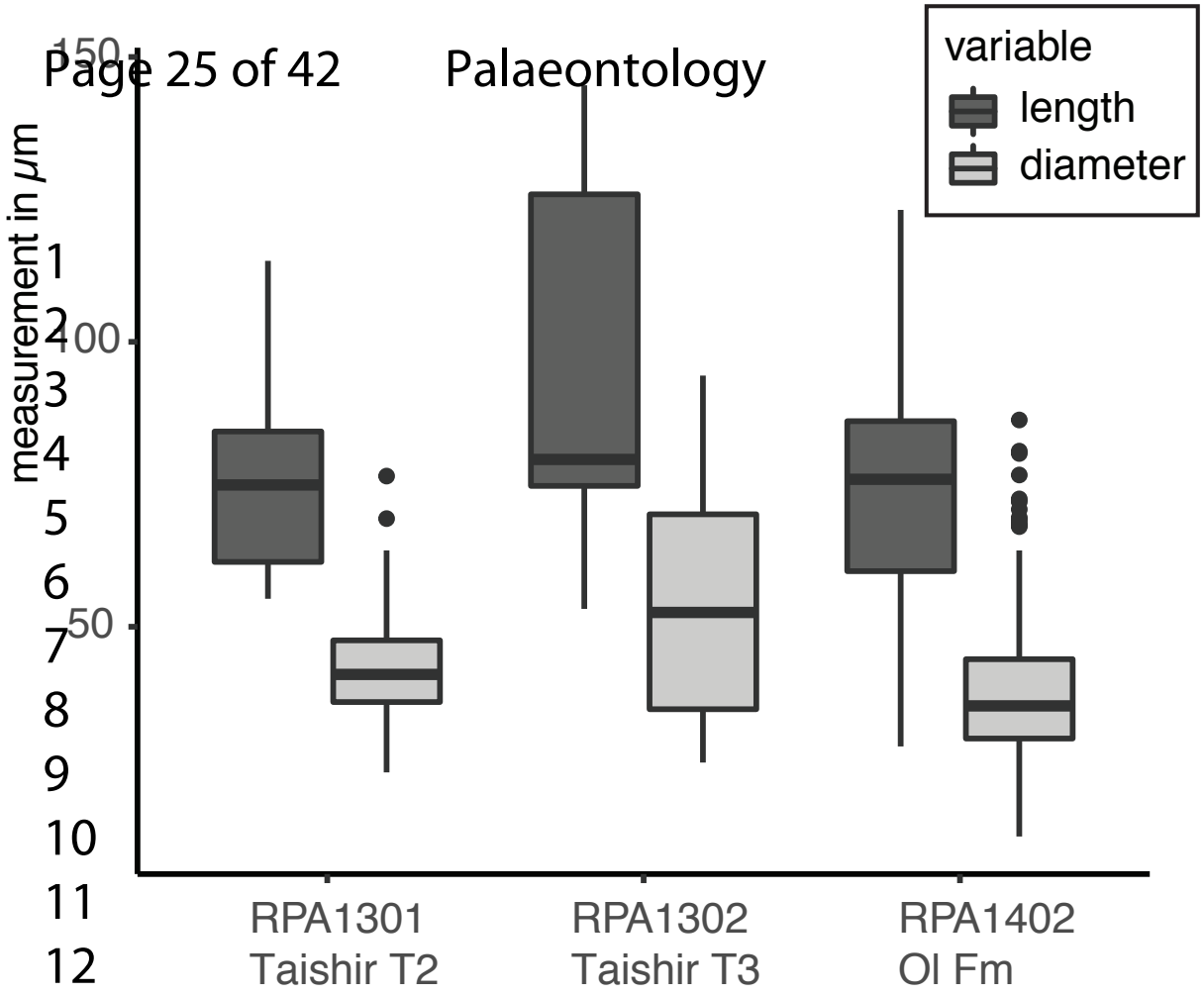
variable
length
diameter
measurement in µm
150
100
50
RPA1301
Taishir T2
RPA1302
Taishir T3
RPA1402
Ol Fm

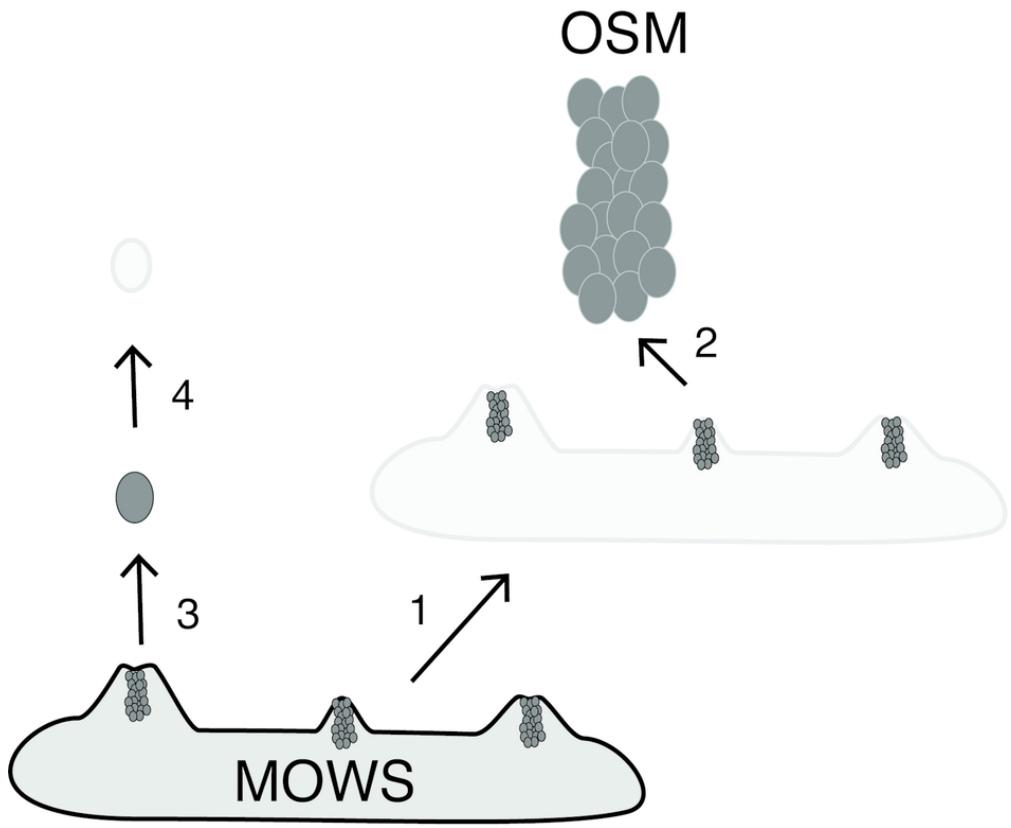

FIG 8. Diagram of potential mechanisms of OSM/MOWS formation and dispersal. 1, External tissues are degraded, leaving behind 2, the internal cellular material as an OSM individual. 3, Carpospores are released, but do not preserve or are lost in sample processing in 4.

80x65mm (300 x 300 DPI)

TABLE 1. MEASUREMENTS OF FOSSIL MATERIAL

Diameters in μm	Mean	Standard Deviation	n	p-value
OSM ends	41.7	15.7	220	
MOWS wart tops	42.1	18.4	107	0.87
OSM cell	3.7	0.99	85	
MOWS wart cell	3.5	0.86	25	0.19

TABLE 2

	Diameter					Length				
	n	Mean	Std	Max	Min	n	Mean	Std	Max	Min
Ol	172	39.3	13.8	86.3	13.2	86	73.7	18.5	123.0	29.0
T2	20	44.3	13.8	76.4	24.4	10	77.2	19.9	114.0	54.9
T3	28	54.9	21.0	94.1	26.2	14	94.0	30.3	145.0	53.1

Feature	Red Algae	Green Algae	Rhizaria	Amoebazoa	sponges
Neoproterozoic fossil and/or molecular clock record	Y	Y	Y	Y	Y
Crustose form	Y	-	-	-	Y
Multicellular & Marine	Y	Y	-	-	Y
Bi-phasic life cycle	Y	Y	-	-	Y
warty protuberances on a single surface	Y	-	-	-	Y
warts contain cellular material	Y	-	-	-	-

ascomycete fungi
Y
Y
-
Y
Y
Y

Member	Locality	Section	Original Mete	BoldMeter	Fossils
Taishir T2	Khongor	F704	128	146.3	MOWS
Taishir T2	Khongor	F704	242	260.3	OSM
Taishir T2	Khongor	F704	328	346.3	OSM
Taishir T2	Khongor	F704	208	226.3	OSM
Taishir T2	Khongor	F704	210	228.3	OSM
Taishir T2	Khongor	F704	242	260.3	OSM
Taishir T3	Khongor	F704	322	340.3	OSM
Taishir T1	Taishir	F713	85	4	OSM
Taishir T2	Taishir	F863	101	289.5	OSM
Taishir T2	Taishir	F864	20	208.5	MOWS
Taishir T2	Taishir	F864	30	218.5	MOWS
Taishir T2	Taishir	F864	30	218.5	OSM
Taishir T2	Taishir	F864	60	248.5	OSM
Taishir T2	Taishir	F864	80	268.5	OSM
Taishir T2	Taishir	F864	121	309.5	OSM
Taishir T3	Taishir	F864	141	329.5	OSM
Taishir T3	Taishir	F865	25	346	MOWS
Taishir T2	Taishir	RPA1301	-1.55	292.4	MOWS
Taishir T2	Taishir	RPA1301	0	293.9	N
Taishir T2	Taishir	RPA1301	-1.37	292.5	N
Taishir T2	Taishir	RPA1301	-2.96	290.9	N
Taishir T2	Taishir	RPA1301	-3.14	290.8	N
Taishir T2	Taishir	RPA1301	-3.8	290.1	N
Taishir T2	Taishir	RPA1301	-5.87	288	N
Taishir T2	Taishir	RPA1301	-5.27	288.6	N
Taishir T2	Taishir	RPA1301	-6.37	287.5	N
Taishir T2	Taishir	RPA1301	-6.67	287.2	N
Taishir T2	Taishir	RPA1301	-7.2	286.7	N
Taishir T2	Taishir	RPA1301	-7.5	286.4	N
Taishir T2	Taishir	RPA1301	-8.02	285.9	N
Taishir T2	Taishir	RPA1301	-8.45	285.5	N
Taishir T2	Taishir	RPA1301	-8.85	285.1	N
Taishir T2	Taishir	RPA1301	-9.28	284.6	N
Taishir T2	Taishir	RPA1301	-9.68	284.2	N
Taishir T2	Taishir	RPA1301	-10.22	283.7	N
Taishir T2	Taishir	RPA1301	-10.75	283.2	N
Taishir T2	Taishir	RPA1301	-11.25	282.7	N
Taishir T2	Taishir	RPA1301	-11.6	282.3	N
Taishir T2	Taishir	RPA1301	-12.45	281.5	N
Taishir T2	Taishir	RPA1301	-13.05	280.9	N
Taishir T2	Taishir	RPA1301	-14.42	279.5	N
Taishir T2	Taishir	RPA1301	-15.18	278.7	N

Taishir T2	Taishir	RPA1301	-15.43	278.5	N
Taishir T2	Taishir	RPA1301	-16.13	277.8	N
Taishir T2	Taishir	RPA1301	-17.08	276.8	N
Taishir T2	Taishir	RPA1301	-11.85	282.1	OSM
Taishir T2	Taishir	RPA1301	-13.75	280.2	OSM
Taishir T2	Taishir	RPA1301	-13.95	280	OSM
Taishir T3	Taishir	RPA1302	0.28	359.5	N
Taishir T3	Taishir	RPA1302	0.68	359.9	N
Taishir T3	Taishir	RPA1302	0.95	360.2	N
Taishir T3	Taishir	RPA1302	1.8	361	N
Taishir T3	Taishir	RPA1302	2.6	361.8	N
Taishir T3	Taishir	RPA1302	2.67	361.9	N
Taishir T3	Taishir	RPA1302	3.02	362.2	N
Taishir T3	Taishir	RPA1302	3.33	362.5	N
Taishir T3	Taishir	RPA1302	3.9	363.1	N
Taishir T3	Taishir	RPA1302	4.1	363.3	N
Taishir T3	Taishir	RPA1302	4.43	363.6	N
Taishir T3	Taishir	RPA1302	4.43	363.6	N
Taishir T3	Taishir	RPA1302	5.11	364.3	N
Taishir T3	Taishir	RPA1302	5.2	364.4	N
Taishir T3	Taishir	RPA1302	5.87	365.1	N
Taishir T3	Taishir	RPA1302	8.37	367.6	N
Taishir T3	Taishir	RPA1302	8.67	367.9	N
Taishir T3	Taishir	RPA1302	11.27	370.5	N
Taishir T3	Taishir	RPA1302	11.87	371.1	N
Taishir T3	Taishir	RPA1302	13.57	372.8	N
Taishir T3	Taishir	RPA1302	13.87	373.1	N
Taishir T3	Taishir	RPA1302	14.95	374.2	N
Taishir T3	Taishir	RPA1302	16.12	375.3	N
Taishir T3	Taishir	RPA1302	17.39	376.6	N
Taishir T3	Taishir	RPA1302	17.45	376.7	N
Taishir T3	Taishir	RPA1302	18.75	378	N
Taishir T3	Taishir	RPA1302	19.53	378.7	N
Taishir T3	Taishir	RPA1302	20.03	379.2	N
Taishir T3	Taishir	RPA1302	22.53	381.7	N
Taishir T3	Taishir	RPA1302	24.75	384	N
Taishir T3	Taishir	RPA1302	25.38	384.6	N
Taishir T3	Taishir	RPA1302	25.98	385.2	N
Taishir T3	Taishir	RPA1302	26.35	385.6	N
Taishir T3	Taishir	RPA1302	27.28	386.5	N
Taishir T3	Taishir	RPA1302	27.9	387.1	N
Taishir T3	Taishir	RPA1302	29.65	388.9	N
Taishir T3	Taishir	RPA1302	1.42	360.6	OSM

Taishir T3	Taishir	RPA1302	2.17	361.4	OSM
Taishir T3	Taishir	RPA1302	7.97	367.2	OSM
Taishir T3	Taishir	RPA1302	9.37	368.6	OSM
Taishir T3	Taishir	RPA1302	28.8	388	OSM
Taishir T3	Taishir	RPA1303	1.16	443.4	MOWS
Taishir T3	Taishir	RPA1303	4.01	446.2	MOWS
Taishir T3	Taishir	RPA1303	10.05	452.3	MOWS
Taishir T3	Taishir	RPA1303	11.65	453.9	MOWS
Taishir T3	Taishir	RPA1303	13.45	455.7	MOWS
Taishir T3	Taishir	RPA1303	1.92	444.1	N
Taishir T3	Taishir	RPA1303	2.5	444.7	N
Taishir T3	Taishir	RPA1303	3.2	445.4	N
Taishir T3	Taishir	RPA1303	3.77	446	N
Taishir T3	Taishir	RPA1303	5.01	447.2	N
Taishir T3	Taishir	RPA1303	5.21	447.4	N
Taishir T3	Taishir	RPA1303	5.41	447.6	N
Taishir T3	Taishir	RPA1303	5.6	447.8	N
Taishir T3	Taishir	RPA1303	6.95	449.2	N
Taishir T3	Taishir	RPA1303	7.8	450	N
Taishir T3	Taishir	RPA1303	8.35	450.6	N
Taishir T3	Taishir	RPA1303	9.25	451.5	N
Taishir T3	Taishir	RPA1303	11.45	453.7	N
Taishir T3	Taishir	RPA1303	12.05	454.3	N
Taishir T3	Taishir	RPA1303	12.95	455.2	N
Taishir T3	Taishir	RPA1303	14	456.2	N
Taishir T3	Taishir	RPA1303	15	457.2	N
Ol	Khongor	RPA1402	0.15	603.4	N
Ol	Khongor	RPA1402	0.17	603.4	N
Ol	Khongor	RPA1402	0.22	603.4	N
Ol	Khongor	RPA1402	0.48	603.7	N
Ol	Khongor	RPA1402	0.95	604.2	N
Ol	Khongor	RPA1402	1.65	604.9	N
Ol	Khongor	RPA1402	2.2	605.4	N
Ol	Khongor	RPA1402	3.25	606.5	N
Ol	Khongor	RPA1402	3.75	607	N
Ol	Khongor	RPA1402	4.25	607.5	N
Ol	Khongor	RPA1402	4.4	607.6	N
Ol	Khongor	RPA1402	4.85	608.1	N
Ol	Khongor	RPA1402	5.25	608.5	N
Ol	Khongor	RPA1402	5.55	608.8	N
Ol	Khongor	RPA1402	9.05	612.3	N
Ol	Khongor	RPA1402	9.55	612.8	N
Ol	Khongor	RPA1402	10.8	614	N

Ol	Khongor	RPA1402	11.1	614.3	N
Ol	Khongor	RPA1402	11.7	614.9	N
Ol	Khongor	RPA1402	11.95	615.2	N
Ol	Khongor	RPA1402	12.55	615.8	N
Ol	Khongor	RPA1402	13.75	617	N
Ol	Khongor	RPA1402	14.55	617.8	N
Ol	Khongor	RPA1402	15.55	618.8	N
Ol	Khongor	RPA1402	15.9	619.1	N
Ol	Khongor	RPA1402	16.7	619.9	N
Ol	Khongor	RPA1402	16.9	620.1	N
Ol	Khongor	RPA1402	17.6	620.8	N
Ol	Khongor	RPA1402	42.9	646.1	N
Ol	Khongor	RPA1402	43.4	646.6	N
Ol	Khongor	RPA1402	43.6	646.8	N
Ol	Khongor	RPA1402	45.75	649	N
Ol	Khongor	RPA1402	49.75	653	N
Ol	Khongor	RPA1402	50.25	653.5	N
Ol	Khongor	RPA1402	50.3	653.5	N
Ol	Khongor	RPA1402	50.8	654	N
Ol	Khongor	RPA1402	53.68	656.9	N
Ol	Khongor	RPA1402	53.76	657	N
Ol	Khongor	RPA1402	54.35	657.6	N
Ol	Khongor	RPA1402	57.5	660.7	N
Ol	Khongor	RPA1402	57.55	660.8	N
Ol	Khongor	RPA1402	1.85	605.1	OSM
Ol	Khongor	RPA1402	1.95	605.2	OSM
Ol	Khongor	RPA1402	2.1	605.3	OSM
Ol	Khongor	RPA1402	2.45	605.7	OSM
Ol	Khongor	RPA1402	3.05	606.3	OSM
Ol	Khongor	RPA1402	3.9	607.1	OSM
Ol	Khongor	RPA1402	10.25	613.5	OSM
Ol	Khongor	RPA1402	18	621.2	OSM
Ol	Khongor	RPA1402	43.85	647.1	OSM
Taishir T1	Khongor	RPA1403	6.1	60.1	MOWS
Taishir T1	Khongor	RPA1403	10.35	64.4	MOWS
Taishir T1	Khongor	RPA1403	10.6	64.6	MOWS
Taishir T1	Khongor	RPA1403	13.75	67.8	MOWS
Taishir T1	Khongor	RPA1403	14.5	68.5	MOWS
Taishir T1	Khongor	RPA1403	20.8	74.8	MOWS
Taishir T1	Khongor	RPA1403	21.7	75.7	MOWS
Taishir T1	Khongor	RPA1403	26	80	MOWS
Taishir T1	Khongor	RPA1403	26.8	80.8	MOWS
Taishir T1	Khongor	RPA1403	0.6	54.6	N

Taishir T1	Khongor	RPA1403	1.4	55.4	N
Taishir T1	Khongor	RPA1403	3.6	57.6	N
Taishir T1	Khongor	RPA1403	4.1	58.1	N
Taishir T1	Khongor	RPA1403	7.35	61.4	N
Taishir T1	Khongor	RPA1403	7.8	61.8	N
Taishir T1	Khongor	RPA1403	10	64	N
Taishir T1	Khongor	RPA1403	10.2	64.2	N
Taishir T1	Khongor	RPA1403	11.7	65.7	N
Taishir T1	Khongor	RPA1403	12.05	66.1	N
Taishir T1	Khongor	RPA1403	12.25	66.3	N
Taishir T1	Khongor	RPA1403	12.6	66.6	N
Taishir T1	Khongor	RPA1403	12.75	66.8	N
Taishir T1	Khongor	RPA1403	14.05	68.1	N
Taishir T1	Khongor	RPA1403	14.1	68.1	N
Taishir T1	Khongor	RPA1403	15.15	69.2	N
Taishir T1	Khongor	RPA1403	16.3	70.3	N
Taishir T1	Khongor	RPA1403	19.1	73.1	N
Taishir T1	Khongor	RPA1403	23.2	77.2	N
Taishir T1	Khongor	RPA1403	24.3	78.3	N
Taishir T1	Khongor	RPA1403	25.25	79.3	N
Taishir T1	Khongor	RPA1403	28.2	82.2	N
Taishir T1	Khongor	RPA1403	28.5	82.5	N
Taishir T1	Khongor	RPA1403	29.1	83.1	N
Taishir T1	Khongor	RPA1403	29.85	83.9	N
Taishir T1	Khongor	RPA1403	30.45	84.5	N
Taishir T1	Khongor	RPA1403	30.9	84.9	N
Taishir T1	Khongor	RPA1403	31.95	86	N
Taishir T1	Khongor	RPA1403	32.35	86.4	N
Taishir T1	Khongor	RPA1403	33.45	87.5	N
Taishir T1	Khongor	RPA1403	34.5	88.5	N
Taishir T1	Khongor	RPA1403	35.15	89.2	N
Taishir T1	Khongor	RPA1403	35.9	89.9	N
Taishir T1	Khongor	RPA1403	38.45	92.5	N
Taishir T1	Khongor	RPA1403	38.8	92.8	N
Taishir T1	Khongor	RPA1403	40.5	94.5	N
Taishir T1	Khongor	RPA1403	41.1	95.1	N
Taishir T1	Khongor	RPA1403	42	96	N
Taishir T1	Khongor	RPA1403	43.1	97.1	N
Taishir T1	Khongor	RPA1403	46.2	100.2	N
Taishir T1	Khongor	RPA1403	46.7	100.7	N
Taishir T1	Khongor	RPA1403	47.8	101.8	N
Taishir T1	Khongor	RPA1403	48.35	102.4	N
Taishir T1	Khongor	RPA1403	49.7	103.7	N

Taishir T1	Khongor	RPA1403	49.8	103.8	N
Taishir T1	Khongor	RPA1403	51.5	105.5	N
Taishir T1	Taishir	RPA1406	3.15	19.5	N
Taishir T1	Taishir	RPA1406	10.2	26.5	N
Taishir T1	Taishir	RPA1406	10.65	27	N
Taishir T1	Taishir	RPA1406	11.65	28	N
Taishir T1	Taishir	RPA1406	12.55	28.9	N
Taishir T1	Taishir	RPA1406	15	31.3	N
Taishir T1	Taishir	RPA1406	18.4	34.7	N
Taishir T1	Taishir	RPA1406	18.75	35.1	N
Taishir T1	Taishir	RPA1406	18.95	35.3	N
Taishir T1	Taishir	RPA1406	22.35	38.7	N
Taishir T1	Taishir	RPA1406	23.15	39.5	N
Taishir T1	Taishir	RPA1406	23.4	39.7	N
Taishir T1	Taishir	RPA1406	27.4	43.7	N
Taishir T1	Taishir	RPA1406	28.9	45.2	N
Taishir T1	Taishir	RPA1406	31.1	47.4	N
Taishir T1	Taishir	RPA1406	47.4	63.7	N
Taishir T1	Taishir	RPA1406	48.95	65.3	N
Taishir T1	Taishir	RPA1406	54.2	70.5	N
Taishir T1	Taishir	RPA1406	127.9	144.2	N
Taishir T1	Taishir	RPA1406	128.6	144.9	N
Taishir T1	Taishir	RPA1406	129	145.3	N
Taishir T1	Taishir	RPA1406	130.3	146.6	N
Taishir T1	Taishir	RPA1406	131	147.3	N
Taishir T1	Taishir	RPA1406	132.3	148.6	N
Taishir T1	Taishir	RPA1406	133.2	149.5	N
Taishir T1	Taishir	RPA1406	134.2	150.5	N
Taishir T1	Taishir	RPA1406	135.8	152.1	N
Taishir T1	Taishir	RPA1406	140.3	156.6	N

Accession #	Reference
	Bosak et al. 2011
	Bosak et al. 2011
	Bosak et al. 2011
	Bosak et al. 2011
	Bosak et al. 2011
	Bosak et al. 2011
	Bosak et al. 2011
	Bosak et al. 2011
	Bosak et al. 2011
	Bosak et al. 2011
	Bosak et al. 2011
	Bosak et al. 2011
	Bosak et al. 2011
	Bosak et al. 2011
	Bosak et al. 2011
	Bosak et al. 2011
	Bosak et al. 2011
YPM IP 547715	This study
	This study
	This study
	This study
	This study
	This study
	This study
	This study
	This study
	This study
	This study
	This study
	This study
	This study
	This study
	This study
	This study
	This study
	This study
	This study
	This study
	This study
	This study
	This study
	This study
	This study
	This study
	This study

	This study
	This study
	This study
YPM IP 547715	This study
YPM IP 547715	This study
YPM IP 547715	This study
	This study
	This study
	This study
	This study
	This study
	This study
	This study
	This study
	This study
	This study
	This study
	This study
	This study
	This study
	This study
	This study
	This study
	This study
	This study
	This study
	This study
	This study
	This study
	This study
	This study
	This study
	This study
	This study
	This study
	This study
	This study
	This study
	This study
	This study
	This study
	This study
YPM IP 547716	This study

YPM IP 547716	This study
YPM IP 547716	This study
YPM IP 547716	This study
YPM IP 547716	This study
YPM IP 547717	This study
YPM IP 547717	This study
YPM IP 547717	This study
YPM IP 547717	This study
YPM IP 547717	This study
	This study
	This study
	This study
	This study
	This study
	This study
	This study
	This study
	This study
	This study
	This study
	This study
	This study
	This study
	This study
	This study
	This study
	This study
	This study
	This study
	This study
	This study
	This study
	This study
	This study
	This study
	This study
	This study
	This study
	This study
	This study
	This study
	This study
	This study

	This study
	This study
	This study
	This study
	This study
	This study
	This study
	This study
	This study
	This study
	This study
	This study
	This study
	This study
	This study
	This study
	This study
	This study
	This study
	This study
	This study
	This study
	This study
	This study
	This study
	This study
YPM IP 547718	This study
YPM IP 547718	This study
YPM IP 547718	This study
YPM IP 547718	This study
YPM IP 547718	This study
YPM IP 547718	This study
YPM IP 547718	This study
YPM IP 547718	This study
YPM IP 547718	This study
YPM IP 547718	This study
YPM IP 547720	This study
YPM IP 547720	This study
YPM IP 547720	This study
YPM IP 547720	This study
YPM IP 547720	This study
YPM IP 547720	This study
YPM IP 547720	This study
YPM IP 547720	This study
YPM IP 547720	This study
	This study

This study
This study
This study
This study
This study
This study
This study
This study
This study
This study
This study
This study
This study
This study
This study
This study
This study
This study
This study
This study
This study
This study
This study
This study
This study
This study
This study
This study
This study
This study
This study
This study
This study
This study
This study
This study
This study
This study
This study
This study
This study
This study
This study

This study
This study
This study
This study
This study
This study
This study
This study
This study
This study
This study
This study
This study
This study
This study
This study
This study
This study
This study
This study
This study
This study
This study
This study
This study
This study
This study
This study
This study
This study
This study
This study
This study
This study
This study